Inorganic Chemistry
Article
pubs.acs.org/IC

Theoretical and Experimental Investigations on Hypoelectronic Heterodimetallaboranes of Group 6 Transition Metals

Bellie Sundaram Krishnamoorthy,[†] Arunabha Thakur,[‡] Kiran Kumar Varma Chakrahari,[‡] Shubhankar Kumar Bose,[‡] Paul Hamon,[†] Thierry Roisnel,[†] Samia Kahlal,[†] Sundargopal Ghosh,*[,‡] and Jean-François Halet*[,†]

[†]Institut des Sciences Chimiques de Rennes, UMR 6226 CNRS-Université de Rennes 1, Avenue du Général Leclerc, 35042 Rennes Cedex, France

[‡]Department of Chemistry, Indian Institute of Technology Madras, Chennai 600 036, India

Supporting Information

ABSTRACT: Density functional theory (DFT) has been used to probe the bonding and electronic properties of dimolybdaborane $[(Cp^*Mo)_2B_5H_9]$, **1** ($Cp^* = \eta^5$-C_5Me_5), and several other heterodimolybdaborane clusters, such as $[(Cp^*Mo)_2B_5(\mu_3\text{-OEt})H_7]$ (**2**), $[(Cp^*Mo)_2B_5(\mu_3\text{-OEt})(n\text{-BuO})H_6]$ (**3**), $[(\eta^5\text{-}C_5H_5W)_2B_4H_4S_2]$ (**4**), and $[(Cp^*Mo)_2B_4H_4E_2]$ (**5**–**7**, where, for **5**, E = S, for **6**, E = Se, and for **7**, E = Te). The DFT results were also used to address some key points such as (i) the metal–metal bond length, (ii) the location and number of bridging and terminal hydrogen atoms, (iii) the molecular orbital analysis, and (iv) the assignment of ^{11}B and ^{1}H NMR chemical shifts. These studies further provide meticulous insight into similarities and differences between various dimetallaborane clusters **1**–**7**. In addition, the crystal structures of **5** and **7** are reported, which come on top of the already existing literature of dimetallaboranes and support the theoretical findings.

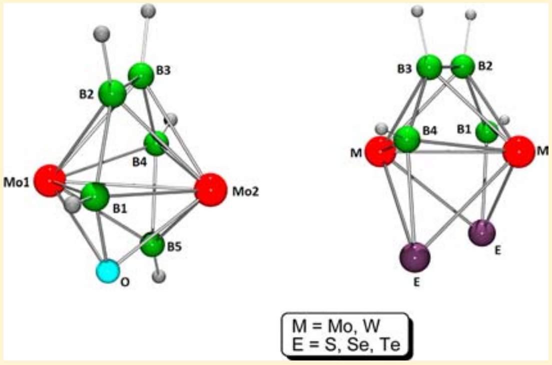

INTRODUCTION

Metallaboranes are often thought as compounds intermediate between borane clusters on one hand and transition-metal complexes on the other.[1] Thus, they provide a test bed for the evaluation of electronic compatibility (or incompatibility) of metal and borane fragments. Among them, dimetallaborane compounds constitute a larger part, since almost one hundred of them are known and have been structurally characterized.[2,3] On the other hand, structures exhibited by dimetallaboranes of the late transition metals often resemble those of the analogous borane and metal clusters. As a result, it turns out that those of earlier transition metals depict specific and unusual shapes generally not defined by either borane or metal cluster systems.[4] Although the experimental metallaborane chemistry is fast growing, theoretical studies are rather scarce.[4,5] In fact, many areas of metallaborane chemistry merit theoretical investigations, viz, (i) structural diversity, (ii) thermal and kinetic stability, (iii) isomeric preferences, (iv) bonding mode, (vi) spectroscopic properties, etc. which can give firm connection with the experimental structural characterization of metallaboranes.

In this paper, we are interested in recent experimental studies on the synthesis of few higher-nuclearity molybdaborane clusters, for example, **1** and two eight-vertex oxamolybdaborane clusters **2** and **3** (see Chart 1).[6] In clusters **2** and **3**, one of the oxygen atoms is contiguously bound to both metal (Mo) and B atoms, exhibiting a cluster connectivity number of three. The crystallographically characterized metallaborane clusters that contain oxygen as part of the cluster core are rare, such as the 10-vertex *nido*-$[(\eta^6\text{-}C_6H_3Me_3)FeOB_8H_{10}]$[7] and *arachno*-$[(PMe_2Ph)_2PtOB_8H_{10}]$[8] species, and 12-vertex *nido*-$[Cp^*RhOB_{10}H_{10}(NEt_3)]$[9] and *nido*-$[Cp^*RhOB_{10}H_9Cl(PMe_2Ph)]$[10] compounds. Until now, compounds **2** and **3** have constituted the first example of oxadimetallaborane clusters containing oxygen as a cluster constituent with a cluster connectivity of three. The Mo–Mo bond lengths in **2** and **3** of 2.638(8) Å and 2.661(7) Å, respectively, are considerably shorter than those observed in cluster **1** (2.808(6) Å).[11] Similarly, the metal–metal bond distances in the heterometallaborane clusters (**4**, **5**, **6**, and **7**, of 2.652(13) Å,[12] 2.633(8) Å, 2.665(2) Å,[13] and 2.692(6) Å, respectively) are also substantially shorter when compared to that in **1**. In addition, significant metal–metal bond shortening has also been observed in oxatantallaborane $[(Cp^*Ta)_2B_4H_{10}O]$[14] (**8**), in comparison to $[(Cp^*Ta)_2(B_2H_6)_2]$.[15] This M–M bond shortening due to the insertion of O, S, Se, and Te atoms to cluster **1** tempted us to carry out a detailed theoretical study using density functional theory (DFT). Furthermore, there are some other interesting aspects to look at: they are the

Received: July 19, 2012
Published: September 17, 2012

Chart 1. Core Geometry of Dimolybdaboranes, 1, 2a, 3a, and 4−7

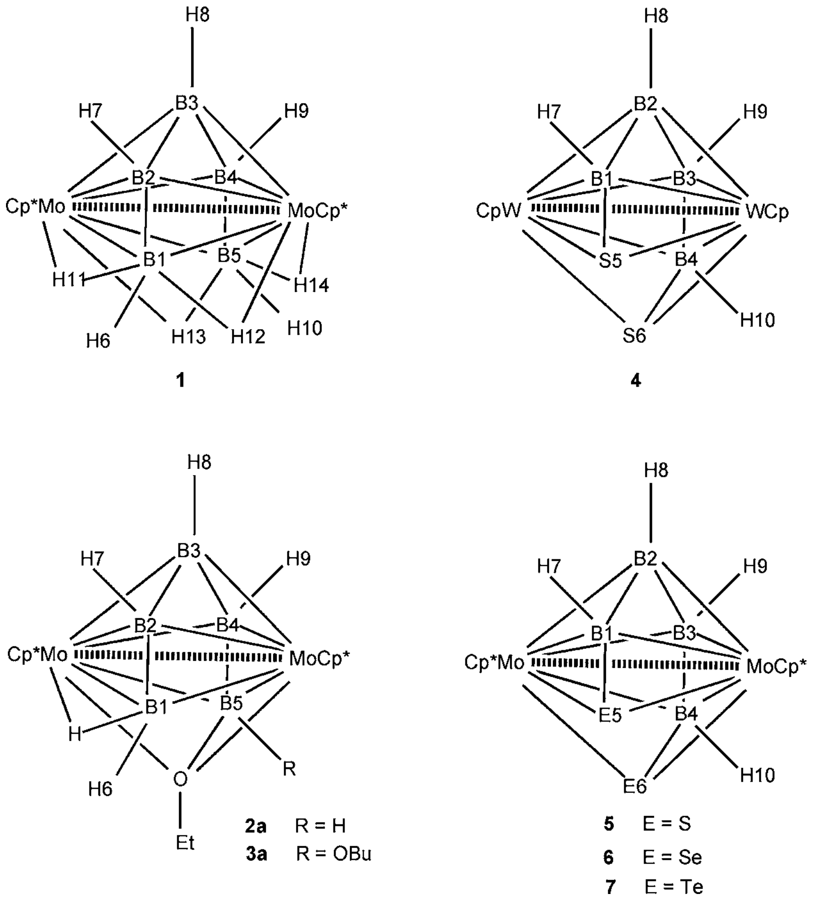

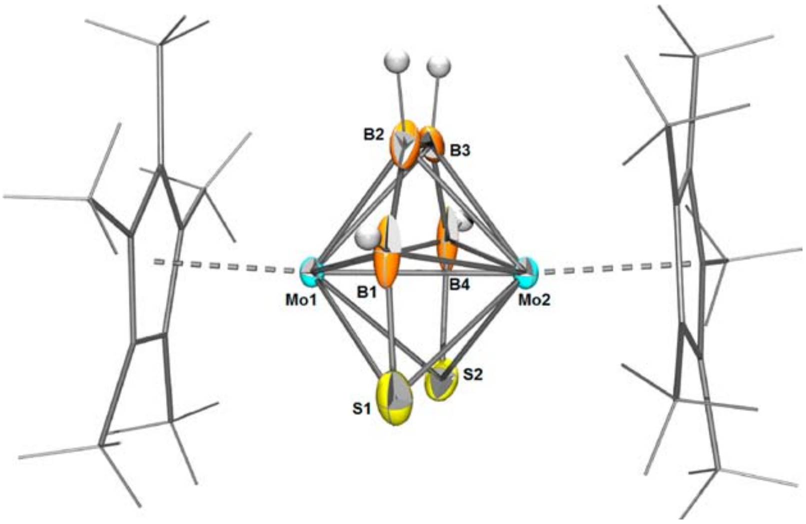

Figure 1. Molecular structure and labeling diagram for **5**. Thermal ellipsoids are shown at the 30% probability level. Selected bond lengths: Mo1−Mo2, 2.633(8) Å, Mo2−B1, 2.383(9) Å, Mo2−B3, 2.233(10) Å, B1−B2, 1.659(18) Å, B2−B3, 1.723(19) Å, B1−S1, 1.855(14) Å, B4−S2, 1.829(15) Å, Mo1−S1, 2.453(2) Å, Mo2−S1, 2.447(2) Å. Selected bond angles: Mo1−B1−Mo2, 67.1(2)°, Mo1−B3−Mo2, 71.9(3)°, Mo1−S1−Mo2, 65.01(6)°.

electronic origins of their unusual shapes within the framework of cluster electron-counting rules in combination with the isolobal analogy,[16−20] which relates the frontier orbitals of main group elements and transition-metal fragments.[21,22] Indeed, computational studies using the ab initio/IGLO/NMR method have been proved to be successful in assigning the bridging H atom location and substitution pattern in boranes and metallaboranes. For example, the experimentally proposed structure of *closo*-1,2-$C_2B_3H_5$, i.e., *closo*-C-3-Me_2-1,2-$C_2B_3H_3$, based on nuclear magnetic resonance (NMR) evidence, was proved to be incorrect on the basis of ab initio/IGLO/NMR calculations.[23] The structures of pentaborane and hexaborane were reconfirmed and refined by theoretical studies.[24]

In this report, with the aid of DFT calculations, we explore the different points mentioned above, viz, the short metal−metal bond, the location and number of bridging and terminal hydrogen atoms and the assignment of ^{11}B and ^{1}H NMR chemical shifts of clusters **1**−**7**. In addition, two new crystal structures **5** and **7**, which are, respectively, sulfur and tellurium analogues of diselenamolybdaborane (**6**)—are reported, which give extra support to the theoretical findings.

RESULTS AND DISCUSSION

Synthesis and Structural Characterization of [$(Cp^*Mo)_2B_4H_4E_2$] (5, E = S; 7, E =Te). The analogy between the bonding properties of certain main-group fragments and transition-metal fragments is an established concept of the bonding in metallaborane systems.[25] The synthesis of main-group element analogue provides an experimental platform for the development and understanding of the role of element variation in both structure and reactivity. After having compounds **5** and **7** in good yields from the reaction of [Cp^*MoCl_4] with $LiBH_4$ at low temperature, followed by thermolysis with chalcogen powder at 110 °C for 30 h, suitable X-ray quality crystals were grown from CH_2Cl_2/hexane solution and that allowed us to get the solid-state structures of **5** and **7**.

The solid-state structures of **5** and **7** confirm the structural inferences made on the basis of spectroscopic data reported earlier.[13] As shown in Figures 1 and 2, both the chalcogen atoms in **5** and **7** are in the open face and bound contiguously to one B atom and two Mo atoms. The Mo−Mo bond length of 2.633(8) Å in **5** is significantly shorter than that observed in the **1** cluster (2.808(6) Å).[11] The Mo−Mo bond length of 2.692(6) Å in **7** is somewhat longer than the corresponding Mo−Mo bond distances in **5** and **6** (2.665(2) Å).[13] As will be discussed in the next section, the significant shortening of the Mo−Mo bond length from Te to S is due to the size and electronegativity effects of S vs Te. All the B−B bond distances in compounds **5** and **7** are in the normal range. The average B−S (1.842 Å) and B-Se bond lengths (1.923 Å) are significantly shorter, compared to those of thiaborane and selenaborane clusters.[26] Similarly, the average B−Te bond length (2.072 Å) in **7** is shorter than the sum of the covalent radii of boron and tellurium (2.18 Å). This may be due to the tendency of boron and chalocogen atoms to form polarized bonds that have a localized two-center character, resulting in the observed distances.[27] The Mo−Te bond lengths (2.766, 2.791, and 2.774 Å) are close to the previously reported Mo−Te bond lengths (2.696(1), 2.816(1), and 2.806(1) Å) in $\{[(Mo_3Te_7(CN)_6]I\}^{3-}$ for instance.[28]

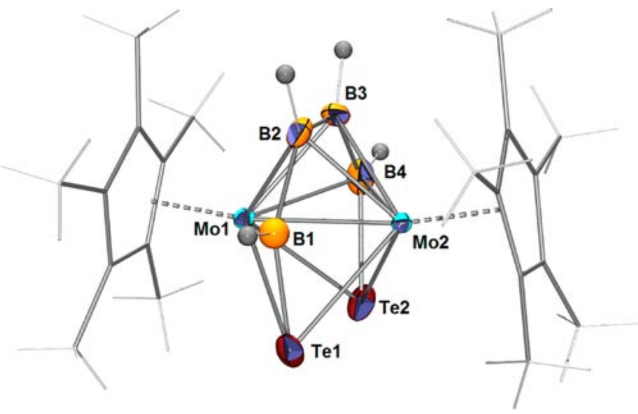

Figure 2. Molecular structure and labeling diagram for **7**. Thermal ellipsoids are shown at the 30% probability level. Selected bond lengths: Mo1−Mo2, 2.692(6) Å; Mo2−B1, 2.409(8) Å; Mo2−B3, 2.241(7) Å; B1−B2, 1.872(17) Å; B2−B3, 1.713(12) Å; B1−Te1, 2.033(11) Å; B4−Te2, 2.112(10) Å; Mo1−Te1, 2.765(6) Å. Selected bond angles: Mo1−B1−Mo2, 73.8(2)°; Mo1−Te1−Mo2, 57.855(16)°.

Geometry Optimizations. Pertinent bond lengths for the all-electron BP86/TZ2P scalar ZORA (zeroth order regular approximation) optimized geometries, along with the X-ray bond parameters, are given in Tables 1 (**1**−**3a**) and 2 (**4**−**7**).

Table 1. Selected Bond Parameters for the Compounds $(Cp^*Mo)_2B_5H_9$ (1), $(Cp^*Mo)_2B_5(\mu_3\text{-OEt})H_6$ (2a), and $(Cp^*Mo)_2B_5(\mu_3\text{−OEt})(n\text{-BuO})H_5$ (3a) Optimized at the BP86/TZ2P Level[a]

	bond lengths (Å)		
atom pair	$(Cp^*Mo)_2B_5H_9$ (**1**)	$(Cp^*Mo)_2B_5$ (μ_3-OEt)H_6 (**2a**)	$(Cp^*Mo)_2B_5(\mu_3$-OEt) (n-BuO)H_5 (**3a**)
Mo12−Mo13	2.810 (2.809)	2.671 (2.638)	2.694 (2.661)
Mo12−B1	2.327 (2.320)	2.169 (2.326)	2.324 (2.381)
Mo12−B2	2.231 (2.214)	2.265 (2.249)	2.181 (2.229)
Mo12−B3	2.213 (2.181)	2.225 (2.227)	2.304 (2.233)
Mo12−B4	2.230 (2.209)	2.305 (2.259)	2.274 (2.265)
Mo12−B5	2.326 (2.322)	2.456 (2.392)	2.630 (2.441)
Mo13−B1	2.327 (2.322)	2.338 (2.363)	2.151 (2.365)
Mo13−B2	2.234 (2.211)	2.215 (2.246)	2.245 (2.211)
Mo13−B3	2.210 (2.176)	2.293 (2.218)	2.197 (2.206)
Mo13−B4	2.232 (2.216)	2.286 (2.268)	2.341 (2.271)
Mo13−B5	2.325 (2.312)	2.486 (2.372)	2.481 (2.425)
B1−B2	1.758 (1.732)	1.753 (1.716)	1.785 (1.728)
B2−B3	1.722 (1.715)	1.688 (1.670)	1.715 (1.655)
B3−B4	1.723 (1.712)	1.689 (1.707)	1.690 (1.675)
B4−B5	1.759 (1.735)	1.668 (1.674)	1.674 (1.707)
$B5−O_{Et}$		1.458 (1.392)	1.450 (1.409)
$B5−O_{Bu}$			1.389 (1.402)

[a] Experimental X-ray analysis values given in brackets.

The computed and experimentally measured bond parameters are in a good agreement for **1** and **4**−**7**. For example, the experimentally observed Mo−Mo distance of 2.808(6) Å in **1** is very close to the calculated one (2.810 Å). In a similar fashion, the calculated Mo−Mo distances for **5**, **6**, and **7**, of 2.629, 2.646, and 2.682 Å, respectively, match well with the experimentally observed respective values of 2.633(8), 2.665(2), and 2.692(6) Å. However, significant deviation was observed for compounds **2** and **3** until their formulas were reconsidered as being [$(Cp^*Mo)_2B_5(\mu_3\text{-OEt})H_6$] (**2a**) instead of [$(Cp^*Mo)_2B_5(\mu_3\text{-OEt})H_7$] (**2**) and [$(Cp^*Mo)_2B_5(\mu_3\text{-OEt})(n\text{BuO})H_5$] (**3a**) instead of [$(Cp^*Mo)_2B_5(\mu_3\text{-OEt})(n\text{BuO})H_6$] (**3**). The formulas of **2** and **3** initially were proposed on the basis of their NMR spectra, assuming that the Mo(2)−B1 bond is doubly H-bridged (Chart 1 for atom numbering).[6] The

Table 2. Selected Bond Parameters for the Compounds (η^5-$C_5H_5W)_2B_4H_4S_2$ (4), $(Cp^*Mo)_2B_4H_4S_2$ (5), $(Cp^*Mo)_2B_4H_4Se_2$ (6) and $(Cp^*Mo)_2B_4H_4Te_2$ (7) Optimized at the BP86/TZ2P Level[a]

atom pair	$(CpW)_2B_4H_4S_2$ (4)	$(Cp^*Mo)_2B_4H_4S_2$ (5)	$(Cp^*Mo)_2B_4H_4Se_2$ (6)	$(Cp^*Mo)_2B_4H_4Te_2$ (7)
		Bond Lengths (Å)		
M11–M12	2.653 (2.653)	2.629(2.633)	2.646 (2.665)	2.682 (2.692)
M11–B1	2.388 (2.357)	2.379(2.390)	2.409 (2.393)	2.427 (2.580)
M11–B2	2.257 (2.223)	2.258(2.249)	2.263 (2.296)	2.264 (2.243)
M11–B3	2.257 (2.228)	2.256(2.259)	2.264 (2.254)	2.268 (2.246)
M11–B4	2.387 (2.350)	2.381(2.384)	2.406 (2.373)	2.423 (2.409)
M12–B1	2.387 (2.350)	2.384(2.389)	2.405 (2.391)	2.422 (2.570)
M12–B2	2.257 (2.228)	2.254(2.246)	2.265 (2.303)	2.268 (2.241)
M12–B3	2.257 (2.223)	2.256(2.244)	2.264 (2.287)	2.264 (2.246)
M12–B4	2.388 (2.357)	2.384(2.369)	2.408 (2.371)	2.427 (2.411)
M11–E5	2.457 (2.448)	2.458(2.453)	2.587 (2.590)	2.806 (2.766)
M11–E6	2.457 (2.451)	2.457(2.444)	2.589 (2.591)	2.808 (2.791)
M12–E5	2.457 (2.451)	2.457(2.447)	2.589 (2.581)	2.808 (2.774)
M12–E6	2.457 (2.448)	2.458(2.449)	2.587 (2.578)	2.806 (2.774)
B1–B2	1.681 (1.597)	1.687(1.659)	1.678 (1.686)	1.665 (1.872)
B2–B3	1.707 (1.715)	1.718(1.745)	1.710 (1.708)	1.701 (1.731)
B3–B4	1.681 (1.597)	1.688(1.677)	1.678 (1.747)	1.665 (1.664)
B1–E5	1.826 (1.859)	1.820(1.857)	1.958 (1.906)	2.155 (2.033)
B4–E6	1.826 (1.859)	1.820(1.828)	1.959 (1.920)	2.155 (2.112)
		Bond Angles (°)		
E5–B1–B2	124.64 (125.21)	125.16(123.74)	127.04 (130.05)	130.81 (121.29)
B1–B2–B3	130.97 (131.18)	130.62(131.32)	131.89 (129.10)	132.75 (135.19)
B2–B3–B4	130.95 (131.18)	130.59(129.87)	131.90 (129.98)	132.78 (131.81)
B3–B4–E6	124.66 (125.21)	125.14(124.73)	127.03 (128.70)	130.80 (130.49)

[a] Experimental X-ray analysis values given in brackets.

geometry optimization of **2** at the BP86/TZ2P all electron scalar ZORA level yielded an Mo–Mo bond length of 2.734 Å, which is 0.11 Å longer than experimentally observed for **2** (2.638(8) Å). However, when one bridging hydride is removed, the BP86/TZ2P optimized structure of **2a** results in a Mo–Mo bond length of 2.671 Å, which is much closer to the experimental value. We thus conclude that compound **2** possesses five terminal H atoms and one Mo–H–B proton (see Chart 1).

Similarly, the geometry optimization of **3** at the BP86/TZ2P all-electron ZORA level shows an Mo–Mo bond length of 2.825 Å, which is significantly longer than the experimentally observed value of 2.661(7) Å. However, the optimization of **3a** at the BP86/TZ2P level resulted in an Mo–Mo bond length of 2.694 Å, which is close to the experimentally observed Mo–Mo bond length. Hence, in a similar fashion, we conclude that the cluster compound **3** (called **3a** in the following, to differentiate the number of hydrogen atoms) possesses four terminal H atoms and one Mo2–H–B1 hydrogen. Interestingly, both the B–O bond lengths in the X-ray structures of **2a** and **3a** are almost equal (B5–O1 = 1.409 Å and B5–O2 = 1.402 Å). It is expected that the *exo*-polyhedral boron–oxygen single bond B5–O2 would be shorter than the B5–O1 bond, where the oxygen atom O1 is involved in a multicenter bonding with the metallaborane cage. This trend is predicted correctly in the DFT optimized geometries with bond lengths of B5–O1 = 1.450 Å and B5–O2 = 1.389 Å. This illustrates that DFT calculations can be helpul in obtaining an accurate number and positions of bridging/terminal hydrides when crystallography fails. Analogously, the 11-vertex diplatinaborane $[(PPh_3)_2(\mu\text{-}PPh_2)Pt_2B_9H_7\text{-}3,9,11\text{-}(OMe)_3]$ was recently reformulated on the basis of DFT calculations.[29]

Electron Count Considerations. Early transition-metal dimetallaboranes often adopt deltahedral geometries. Although they have the same total connectivity of the classic set of corresponding borane or late-transition-metal metallaborane deltahedra, they are distinctly oblate (flattened along the M–M axis)[30] rather than closely spherical.[4] In addition, these dimetallaborane clusters are generally characterized by metal–metal cross-cluster distances and *apparent* formal cluster electron counts a few skeletal electron pairs (sep) less (generally three) than required for a canonical *closo*-structure of the same nuclearity. The DFT calculations suggested that these hypoelectronic arrangements are very stable compounds, obtained via an intricate mutual interaction of the dimetal fragment and borane cage. Indeed, bringing two CpM or Cp*M (Cp = η^5-C_5H_5) fragments together generates a set of three frontier orbitals that can only interact with the frontier orbitals of a flattened, distinctly ring-like borane fragment. These orbitals on each of these complementary fragments, which normally would be filled in a late transition-metal metallaborane in a spherical deltahedra shape, interact strongly to generate three low-lying filled orbitals and three high-lying unfilled orbitals. As a result, they generate the metal–metal cross-cluster bonding where the effective sep counts are three seps larger than the apparent sep count obtained via the classical Polyhedral Skeletal Electron Pair Theory (PSEPT).[1,4,5]

If the classical skeletal electron counting formalism is applied, cluster **1** can be viewed as an electron-deficient *nido* species derived from an 8-vertex *closo* hexagonal bipyramidal cluster, such as 6-sep $[(Cp^*Re)_2B_6H_4Cl_2]$.[4] Similarly, clusters **2a–7** can be viewed as a 9-vertex *closo* heptahedral bipyramidal cluster by the removal of one boron vertex. Indeed, cluster **1** possesses an *apparent* sep count of 6 [−1(Cp*Mo) × 2 + 2(BH) × 5 + 1(bridging H) × 4/2]. On the other hand, both

Table 3. DFT-Calculated (BP86/TZ2P All-Electron Scalar ZORA Level) Energies of the HOMO and LUMO and HOMO−LUMO Gaps for Complexes 1−7

	1	2a	3a	4	5	6	7
HOMO (eV)	−4.661	−3.837	−3.708	−5.169	−4.579	−4.460	−4.470
LUMO (eV)	−2.248	−1.957	−1.982	−2.891	−2.524	−2.531	−2.64
ΔE (eV)	2.413	1.880	1.726	2.278	2.049	1.929	1.830

of the Mo_2B_4O species, **2a** and **3a** [[−1(Cp*Mo) × 2 + 2(BH/BO) × 5 + 1(bridging H) × 1 + 5(OEt) × 1]/2] and the $M_2B_4E_2$, as well as the **4**−**7** (M = Mo, W and X = S, Se, Te) species [[−1(CpW/Cp*Mo) × 2 + 2(BH) × 4 + 4(S/Se/Te) × 2]/2] possess 7 sep.

Electronic Structure Analysis. DFT molecular orbital diagrams of compounds **1**−**7** are studied and analyzed (see Table 3). The considerable highest occupied molecular orbital−lowest unoccupied molecular orbital (HOMO−LUMO) energy gap computed at the BP86 level for each compound, ca. 2 eV, is consistent with their stability. The composition of the MOs located in the HOMO region reflects strong delocalization over the entire cluster cage, as generally observed for this type of metallaborane.[4] From this study, two observations can be made: for example, (i) the introduction of π-donor chalcogens in the cage induces a destabilization of the HOMO and, consequently, the more electronegative the chalcogen, the smaller the HOMO−LUMO gap, and (ii) the change of Mo atom to the heavier Group 6 analogue, i.e., W (tungsten) shows some substantial stabilization of the HOMO, leading to a larger HOMO−LUMO gap.

Metal−Metal Bonding Analysis (ELF Function). The nature of bonding between the metal atoms in **1**, **2a**, **3a**, and **4**−**7** can be provided by the analysis of the electron localization function (ELF).[31−33] The values are defined between 0 and 1. In general, a value of 0.5 is observed for the homogeneous electron gas; a value equal to 1 indicates a perfect localization, whereas a value of <0.5 indicate a delocalization in a low-density region.

The two-dimensional (2D) electron density distribution plot of compounds **1**, **3a**, and **5** are shown and compared in Figure 3. The ELF plot of compound **1** shows significant delocalization of electron density between the Mo atoms, revealing weak metal−metal interaction; this is in agreement with the long Mo−Mo bond length of 2.809 Å. Consistent with the significant shortening of the Mo−Mo bond length in the chalcogen-containing compounds **3a** and **5**, the ELF value is now higher than 0.5, showing some enhanced electron density between the metal atoms (see Figure 3). The same conclusion is expected for compounds **2a**, **6**, and **7**.

Bond Multiplicities. As listed in Tables 4 and 5, the stronger Mo−Mo interaction in **2a**, **3a**, and **5**−**7**, with respect to **1**, is supported by the DFT-calculated bond multiplicity (BM) indices based on the Nalewajski−Mrozek method.[34] In the case of compounds **4**−**7**, the M−M bond multiplicities slightly decrease, with respect to the increasing size of the chalcogen atoms. In the same compounds, the boron−chalcogen bond multiplicities are ca. 1.2, indicating a strong bonding character. They also decrease very slightly, with respect to the size of the attached chalcogen atom. Interestingly, the computed bond multiplicity of Mo−B5 bond in **2a** is very small (0.34), when compared to those of other M−B bonds. This may be due to the additional binding of the OEt group to the B5 atom. In the case of **3a**, the Mo−B5 bond multiplicity is even lower (0.18), because of the binding of both the OEt and OBu groups to the B5 atom. Noteworthy, the bond multiplicity values for the B5−OEt and B5−OBu—0.99 and 1.29, respectively—indicate a stronger bonding character between the B5 and OBu groups.

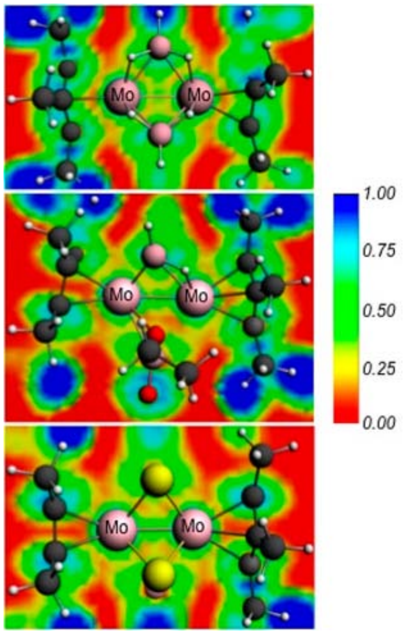

Figure 3. ELF plots (DFT) for compounds **1** (top), **3a** (middle), and **5** (bottom) in the Mo−C(Cp)−Mo plane.

Ionization Potentials (IP). The ionization potential (IP) energies, which are a realistic indicator of the metal−boron cage stability, were computed for all the compounds studied in this work. Both the DFT-computed vertical and adiabatic first IPs are plotted in Figure 4. The computed IP values above 5.0 eV are consistent with the high thermodynamical stability of the compounds studied. The vertical curve is a few tenths of an electronvolt higher in energy, relative to the adiabatic one, because of the significant geometry change upon ionization.

NMR Chemical Shifts. The ^{11}B and ^{1}H NMR chemical shifts with the scalar relativistic ZORA method available in ADF were calculated using both BP86 and B3LYP functionals (see computational details) and compared to the experimental values of clusters **1**−**7**. They are listed in Tables 6 and 7 (see Chart 1 for the atom numbering). Good agreement has been observed both for ^{1}H and ^{11}B chemical shift values (maximum deviations of 3 ppm for ^{1}H NMR and 20 ppm for ^{11}B NMR at BP86/TZ2P level). The values obtained from B3LYP/TZ2P calculations are, in general, slightly closer to the experimentally observed ones with a maximum deviation of ca. 10 ppm for all the boron atoms except B3 (17 ppm) and B5 (40 ppm) in compound **3a** (see below). Pleasingly, the computations allow one to distinguish not only the difference in vertex connectivity (3 vs 4) but also the different environment of every boron atom. Indeed, the presence or absence of bridging hydrogen atoms, the number of direct metal−boron, boron−boron, and/

Table 4. DFT-Calculated (BP86/TZ2P All-Electron Basis Set) Bond Multiplicities (Nalewajski−Mrozek)[33] for the Compounds $(Cp^*Mo)_2B_5H_9$ (1), $(Cp^*Mo)_2B_5(\mu_3\text{-}OEt)H_6$ (2a), and $(Cp^*Mo)_2B_5(\mu_3\text{-}OEt)(n\text{-}BuO)H_5$ (3a)

	bond multiplicity		
atom pair	$(Cp^*Mo)_2B_5H_9$ (**1**)	$(Cp^*Mo)_2B_5(\mu_3\text{-}OEt)H_6$ (**2a**)	$(Cp^*Mo)_2B_5(\mu_3\text{-}OEt)(n\text{-}BuO)H_5$ (**3a**)
Mo12−Mo13	0.67	0.70	0.71
Mo12−B1	0.41	0.95	0.41
Mo12−B2	0.61	0.53	0.74
Mo12−B3	0.58	0.60	0.48
Mo12−B4	0.61	0.43	0.59
Mo12−B5	0.41	0.34	0.18
Mo13−B1	0.41	0.40	0.97
Mo13−B2	0.60	0.68	0.56
Mo13−B3	0.58	0.50	0.64
Mo13−B4	0.60	0.52	0.40
Mo13−B5	0.41	0.31	0.25
B1−B2	0.81	0.79	0.73
B2−B3	0.82	0.86	0.80
B3−B4	0.82	0.93	0.95
B4−B5	0.80	1.06	0.97
$B5{-}O_{Et}$		1.03	0.99
$B5{-}O_{Bu}$			1.29

or heteroelement−boron bonds, the metal identity, and the coordination number might all be important in determining the boron chemical shifts.[35]

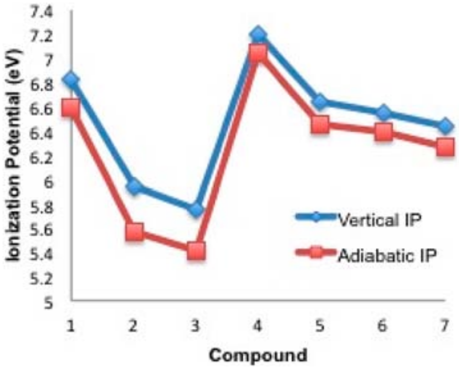

Figure 4. Vertical and adiabatic first ionization potentials (IPs, in eV) for compounds **1**, **2a**, **3a**, and **4**−**7** computed at the BP86/TZ2P all-electron scalar ZORA level.

A close examination of the results, listed in Tables 6 and 7, allows us to draw the following conclusions. Four-vertex-connect boron atoms (2 metal and 2 boron neighbors, i.e., B2, B3 and B4 in **1**, **2a**, and **3a** and B2 and B3 in **4**−**7**) exhibit resonances at low field in the range of 30−90 ppm. The replacement of one boron neighbor by a chalcogen atom in compounds **2a**-**7** leads to a large upfield shift in the range of 11 to (−29) ppm (see B5 for **2a** and **3a** and B1 and B4 for **4**−**7** in Tables 3 and 4).

The calculated and experimental chemical shift values of B4 and B5 in compounds **2a** and **3a**, respectively, vary significantly (0.6 vs 50.8 ppm and 87.5 initially reported[6] vs 6.6 ppm, respectively, at the BP86/TZ2P level). The B4 atom in **2a** is four vertex-connected to two metals and two boron atoms, whereas the B5 atom in **3a** is four vertex-connected to two metals, one boron, and one oxygen atom. With respect to this vertex connectivity and environment, one would expect a chemical shift of boron (B4) in the low-field region for compound **2a**. On the other hand, the chemical shift for this B5 atom in compound **3a** is expected to be appear in the upfield shift region. However, the experimental values differ from the

Table 5. DFT-Calculated (BP86/TZ2P All-Electron Basis Set) Bond Multiplicities (Nalewajski−Mrozek)[33] for the Compounds $(\eta^5\text{-}C_5H_5W)_2B_4H_4S_2$ (4), $(Cp^*Mo)_2B_4H_4S_2$ (5), $(Cp^*Mo)_2B_4H_4Se_2$ (6), and $(Cp^*Mo)_2B_4H_4Te_2$ (7)

	bond multiplicity			
atom pair	$(CpW)_2B_4H_4S_2$ (**4**)	$(Cp^*Mo)_2B_4H_4S_2$ (**5**)	$(Cp^*Mo)_2B_4H_4Se_2$ (**6**)	$(Cp^*Mo)_2B_4H_4Te_2$ (**7**)
M11−M12	0.84	0.79	0.78	0.75
M11−B1	0.45	0.42	0.41	0.43
M11−B2	0.58	0.55	0.54	0.54
M11−B3	0.58	0.55	0.54	0.53
M11−B4	0.45	0.42	0.41	0.43
M12−B1	0.45	0.41	0.42	0.43
M12−B2	0.58	0.55	0.54	0.53
M12−B3	0.58	0.55	0.54	0.54
M12−B4	0.45	0.41	0.42	0.43
M11−E5	0.67	0.62	0.61	0.60
M11−E6	0.67	0.62	0.61	0.59
M12−E5	0.67	0.62	0.61	0.59
M12−E6	0.67	0.62	0.61	0.60
B1−B2	0.94	0.92	0.95	0.97
B2−B3	0.84	0.82	0.83	0.81
B3−B4	0.94	0.92	0.95	0.97
B1−E5	1.19	1.22	1.18	1.16
B4−E6	1.19	1.23	1.18	1.16

Table 6. DFT BP86/TZ2P and B3LYP/TZ2P Computed (Scalar ZORA) and Experimental NMR Chemical Shifts δ (ppm) for the Compounds $(Cp^*Mo)_2B_5H_9$ (1), $(Cp^*Mo)_2B_5(\mu_3\text{-OEt})H_6$ (2a), and $(Cp^*Mo)_2B_5(\mu_3\text{-OEt})(n\text{-BuO})H_5$ (3a)

	$(Cp^*Mo)_2B_5H_9$ (1)			$(Cp^*Mo)_2B_5H_6(\mu_3\text{-OEt})$ (2a)[a]		$(Cp^*Mo)_2B_5H_5(\mu_3\text{-OEt})(n\text{-OBu})$ (3a)		
	Exp.	BP86/TZ2P	B3LYP/TZ2P	Exp.	BP86/TZ2P	Exp	BP86/TZ2P	B3LYP/TZ2P
^{11}B NMR								
B1	28.40	21.31	29.98	68.95	68.64	103.63	78.41	97.26
B2	65.60	50.60	66.46	60.26	54.29	89.25	69.91	86.88
B3	65.60	47.91	61.80	34.81	26.74	33.23	40.38	50.81
B4	65.60	51.13	67.18	0.61	50.83	33.23	32.87	43.98
B5	28.40	21.58	30.24	−4.50	−4.43	−29.30	6.58	12.86
^{1}H NMR								
H6	5.01	3.89	4.15	3.99	6.97	7.56	7.20	7.80
H7	5.61	4.01	4.52	3.58	3.34	2.72	3.76	4.26
H8	3.43	2.35	2.50	3.50	2.27	2.72	2.81	2.88
H9	5.61	4.09	4.60	3.93	6.49	4.10	5.70	5.83
H10	5.01	3.84	4.11	2.18	2.18	−2.56	−0.39	−0.01
H11	−6.84	−7.22	−6.95	−7.15	−1.58			
H12	−6.84	−7.15	−6.89					
H13	−6.84	−7.28	−7.06					
H14	−6.84	−7.28	−7.05					
H(Cp*)	1.93	1.71	1.69	1.90	1.03	1.51	1.91	1.97

[a] B3LYP/TZ2P values could not be computed.

Table 7. DFT BP86/TZ2P and B3LYP/TZ2P Computed (Scalar ZORA) and Experimental NMR Chemical Shifts δ(ppm) for the Compounds $(\eta^5\text{-}C_5H_5W)_2B_4H_4S_2$ (4), $(Cp^*Mo)_2B_4H_4S_2$ (5), $(Cp^*Mo)_2B_4H_4Se_2$ (6), and $(Cp^*Mo)_2B_4H_4Te_2$ (7)

	$(CpW)_2B_4H_4S_2$ (4)			$(Cp^*Mo)_2B_4H_4S_2$ (5)			$(Cp^*Mo)_2B_4H_4Se_2$ (6)			$(Cp^*Mo)_2B_4H_4Te_2$ (7)		
	Exp.	BP86/ TZ2P	B3LYP/ TZ2P	Exp.	BP86/ TZ2P	B3LYP/ TZ2P	Exp.	BP86/ TZ2P	B3LYP/ TZ2P	Exp.	BP86/ TZ2P	B3LYP/ TZ2P
^{11}B NMR												
B1	−10.60	−26.09	−19.54	−4.10	−16.11	−8.52	4.20	−9.24	−1.69	11.60	−0.06	7.02
B2	74.90	62.53	76.94	81.80	73.32	90.45	81.80	73.09	90.30	81.30	75.44	92.39
B3	74.90	62.39	76.77	81.80	73.48	90.13	81.80	73.12	90.13	81.30	75.33	92.22
B4	−10.60	−26.08	−19.55	−4.10	−16.11	−9.64	4.20	−9.30	−2.14	11.60	0.01	6.85
^{1}H NMR												
H7	4.31	0.67	0.60	4.12	0.78	0.62	4.25	1.17	1.11	4.36	1.73	1.56
H8	8.42	5.96	6.30	9.35	6.03	6.47	9.36	6.16	6.62	9.27	6.27	6.76
H9	8.42	5.95	6.29	9.35	5.99	6.54	9.36	6.15	6.58	9.27	6.28	6.79
H10	4.31	0.68	0.60	4.12	0.68	0.67	4.25	1.17	1.06	4.36	1.76	1.66
H(Cp*)	5.69	5.06	4.95	1.94	1.35	1.07	1.92	1.47	1.76	1.93	1.82	1.73

expected values. This important disagreement between experiment and theory led us to reconsider the experimental ^{11}B chemical shift assignment of compounds **2a** and **3a**. Interestingly, an additional peak at −29.3 ppm was observed for **3a** when a careful analysis of ^{11}B NMR was recorded with long scan and at high concentration of **3a**. Although the computed and experimental values are, in general, expected to be in the upfield region, they deviate by ca. 35 ppm at the BP86/TZ2P level and 40 ppm at the B3LYP/TZ2P level. Therefore, this chemical shift has been tentatively assigned to the B5 atom in **3a**.

■ CONCLUSIONS

The present study has proved the strength of theoretical methods to characterize the electronic properties of hypoelectronic heterodimetallaboranes of early transition metals. In particular, DFT calculations show that the molecular formula of the early reported compounds $[(Cp^*Mo)_2B_5(\mu_3\text{-OEt})H_7]$ (**2**) and $[(Cp^*Mo)_2B_5(\mu_3\text{-OEt})(n\text{BuO})H_6]$ (**3**) must indeed be reformulated as $[(Cp^*Mo)_2B_5(\mu_3\text{-OEt})H_6]$ (**2a**) and $[(Cp^*Mo)_2B_5(\mu_3\text{-OEt})(n\text{-BuO})H_5]$ (**3a**), respectively. Compound **1** can be considered as a 6-sep 7-vertex *oblatonido* M_2B_5 cluster derived from the 8-vertex *oblatocloso* M_2B_6 cluster, whereas compounds **2a**, **3a**, and **4**–**7** can be viewed as 7-sep 8-vertex *oblatonido* $M_2B_5O/M_2B_4E_2$ clusters derived from a 9-vertex *oblatocloso* heptagonal bipyramidal cluster by removal of one equatorial boron atom. Furthermore, the DFT method is proved to be helpful in predicting the stability, geometry, electronic structure of these clusters and the assignment of the ^{1}H and ^{11}B NMR chemical shift values.

■ EXPERIMENTAL SECTION

DFT Computational Details. Density functional theory (DFT) calculations were carried out using the Amsterdam Density Functional (ADF) program[36] developed by Baerends and co-workers.[37] The Vosko–Wilk–Nusair parametrization[38] was used for the local density approximation (LDA) with gradient corrections for exchange (Beck88)[39,40] and correlation (Perdew86).[41] The geometry optimization procedure was based on the method developed by Versluis and Ziegler.[42] Relativistic corrections were added using the ZORA scalar Hamiltonian.[43] Structures are initially optimized using the TZP basis set, which is available in the ADF program, by taking experimental geometries as inputs. Furthermore, the BP86/TZP optimized geometries are used as inputs for the optimization and NMR computations using an all-electron TZ2P basis set[36,37] at the relativistic scalar ZORA level of calculations. NMR chemical shifts were also calculated with the hybrid Becke−Lee−Yang−Parr (B3LYP) functional,[44] using the BP86/TZ2P optimized geometries. Computation of the NMR shielding tensors employed gauge-including atomic orbitals (GIAOs),[45−48] using the implementation of Schreckenbach, Wolff, Ziegler, and co-workers.[49−53] The projected ^{11}B chemical shielding values, determined from relativistic scalar ZORA calculations, were referenced to B_2H_6 as the primary reference point, and these chemical shift values (δ) were then converted to the standard BF_3:OEt_2 scale using the experimental value of +16.6 ppm for B_2H_6. The computation of electron localization function (ELF) was done using the ADF-utility program DENSF and visualized with the ADF-GUI module.[36] The chemical bonding of the studied complexes was examined by the Nalewajski−Mrozek bond order method[33] implemented in the ADF program.[36]

X-ray Structure Determination. The crystal structure of **5** was solved by direct methods using the SIR97 program,[54] and then refined with full-matrix least-squares methods based on F^2 (SHELXL-97)[55] with the aid of the WINGX program.[56] All non-hydrogen atoms were refined with anisotropic atomic displacement parameters. H atoms were finally included in their calculated positions. The crystal data for **7** were collected and integrated using a Bruker Axs kappa apex2 CCD diffractometer, with graphite monochromated Mo Kα (λ = 0.71073 Å) radiation at 173 K. The structures were solved by heavy atom methods using SHELXS-97 or SIR92[57] and refined using SHELXL-97.[58]

Crystal data for **5** ($C_{20}H_{34}B_4Mo_2S_2$): crystal system, space group: monoclinic $P2_1/n$. Unit-cell dimensions: a = 15.1781(3) Å, b = 32.3410(7) Å, c = 16.5167(3) Å, β = 114.6850(10)°, V = 7366.7(3) Å^3; Z = 4. Density (d) = 1.552 g cm^{-3}; μ = 1.196 mm^{-1}; final R indices [$I > 2\sigma(I)$] R1 = 0.0721, $wR2$ = 0.1841 (all data). Index ranges: $-13 \le h \le 13$, $-10 \le k \le 10$, $-13 \le l \le 12$. Reflections collected, 4254; independent reflections, 3884, R_{int} = 0.0410; wR_2 = 0.0925 ($I > 2\sigma(I)$); goodness-of-fit on F^2, 1.046.

Crystal data for **7** ($C_{20}H_{34}B_4Mo_2Te_2$): crystal system, space group: orthorhombic, $Pbca$. Unit-cell dimensions: a = 15.8507(3) Å, b = 14.7628(3) Å, c = 21.2848(4) Å, β = 96.6590(10)°; Z = 8. Density (calculated) = 2.040 Mg/m^3. Final R indices [$I > 2\sigma(I)$] R1 = 0.0633, $wR2$ = 0.1452 (all data). Index ranges: $-22 \le h \le 18$, $-20 \le k \le 17$, $-29 \le l \le 29$. Reflections collected 7259, independent reflections 5844, R_{int} = 0.0514; wR_2 = 0.1408 ($I > 2\sigma(I)$); goodness-of-fit on F^2, 1.056.

■ ASSOCIATED CONTENT

Ⓢ Supporting Information

X-ray crystallographic files in CIF format for **5** and **7**. The optimized geometries of all the structures studied (Cartesian coordinates, in Å). This material is available free of charge via the Internet at http://pubs.acs.org.

■ AUTHOR INFORMATION

Corresponding Author

*E-mail addresses: sghosh@iitm.ac.in (S.G.), halet@univ-rennes1.fr (J.-F.H.).

Notes

The authors declare no competing financial interest.

■ ACKNOWLEDGMENTS

Generous support of the Indo-French Centre for the Promotion of Advanced Research (IFCPAR-CEFIPRA), No. 4405-1, New Delhi is gratefully acknowledged. A.T. and K.K.V.C. thank the Council of Scientific and Industrial Research and University Grants Commission, India, for research fellowships.

■ REFERENCES

(1) Fehlner, T. P.; Halet, J.-F.; Saillard, J.-Y.: *Molecular Clusters. A Bridge to Solid-State Chemistry*; Cambridge University Press: New York, 2007.

(2) Fehlner, T. P. *Organometallics* **2000**, *19*, 2643.

(3) King, R. B. *Inorg. Chem.* **2004**, *43*, 4241.

(4) Le Guennic, B.; Jiao, H.; Kahlal, S.; Saillard, J.-Y.; Halet, J.-F.; Ghosh, S.; Shang, M.; Beatty, A. M.; Rheingold, A. L.; Fehlner, T. P. *J. Am. Chem. Soc.* **2004**, *126*, 3203.

(5) Bose, S. K.; Ghosh, S.; Noll, B. C.; Halet, J.-F.; Saillard, J.-Y.; Vega, A. *Organometallics* **2007**, *26*, 5377.

(6) Sahoo, S.; Dhayal, R. S.; Varghese, B.; Ghosh, S. *Organometallics* **2009**, *28*, 1586.

(7) Micciche, R. P.; Briguglio, J. J.; Sneddon, L. G. *Inorg. Chem.* **1984**, *23*, 3992.

(8) Kim, Y.-H.; Brownless, A.; Cooke, P. A.; Greatrex, R.; Kennedy, J. D.; Thornton-Pett, M. *Inorg. Chem. Commun.* **1998**, *1*, 19.

(9) Ditzel, E. J.; Fontaine, X. L. R.; Fowkes, H.; Greenwood, N. N.; Kennedy, J. D.; MacKinnon, P.; Sisan, Z.; Thornton-Pett, M. *J. Chem. Soc. Chem. Commun.* **1990**, 1692.

(10) Fontaine, X. L. R.; Fowkes, H.; Greenwood, N. N.; Kennedy, J. D.; Thornton-Pett, M. *J. Chem. Soc., Chem. Commun.* **1985**, 1722.

(11) Kim, D. Y.; Girolami, G. S. *J. Am. Chem. Soc.* **2006**, *108*, 10969.

(12) Dhayal, R. S.; Ponniah, S. J.; Sahoo, S.; Ghosh., S. *Indian J. Chem.* **2011**, *50A*, 1363.

(13) Sahoo, S.; Mobin, S. M.; Ghosh, S. *J. Organomet. Chem.* **2010**, *695*, 945.

(14) Bose, S. K.; Geetharani, K.; Sahoo, S.; Reddy, K. H. K.; Varghese, B.; Jemmis, E. D.; Ghosh, S. *Inorg. Chem.* **2011**, *50*, 9414.

(15) Bose, S. K.; Geetharani, K.; Ramkumar, V.; Mobin, Sk. M.; Ghosh, S. *Chem.—Eur. J.* **2009**, *15*, 13483.

(16) Wade, K. *Inorg. Nucl. Chem. Lett.* **1972**, *8*, 559.

(17) Wade, K. *Adv. Inorg. Chem. Radiochem.* **1976**, *18*, 1.

(18) Mingos, D. M. P. *Nature (London) Phys. Sci.* **1972**, *236*, 99.

(19) Mingos, D. M. P. *Acc. Chem. Res.* **1984**, *17*, 311.

(20) Mingos, D. M. P.; Wales, D. J. *Introduction to Cluster Chemistry*; Prentice Hall: New York, 1990.

(21) Hoffmann, R. *Science* **1981**, *211*, 995.

(22) Hoffmann, R. *Angew. Chem., Int. Ed. Engl.* **1982**, *21*, 711.

(23) Onak, T. P.; Williams, R. E. *Inorg. Chem.* **1994**, *33*, 5471.

(24) Buhl, M.; Schleyer, P. v. R. in *Electron Deficient Boron and Carbon Clusters*; Olah, G. A., Wade, K., Williams, R. E., Eds.; Wiley: New York, 1991; Chapter 4, p 113.

(25) Mingos, D. M. P. *J. Chem. Soc., Dalton Trans.* **1974**, 133.

(26) (a) Norman, N. C.; Orpen, A. G.; Quayle, M. J.; Rice, C. R. *New J. Chem.* **2000**, *24*, 837. (b) Hammerschmidt, A.; Döch, M.; Pütz, S.; Krebs, B. *Z. Anorg. Allg. Chem.* **2005**, *631*, 1125.

(27) (a) Bicerano, J.; Lipscomb, W. N. *Inorg. Chem.* **1980**, *19*, 1825. (b) Dolansky, J.; Hermanek, S.; Zahradnik, R. *Collect. Czech. Chem. Commun.* **1981**, *46*, 2479.

(28) Fedin, V. P.; Imoto, H.; Saito, T.; McFarlane, W.; Sykes, G. *Inorg. Chem.* **1995**, *34*, 5097.

(29) Nie, Y.; Miao, J.-L.; Hu, C.-H.; Chen, H.-Y.; Cheung, M. S.; Lin., Z.-Y.; Enders, M.; Siebert, W. *Polyhedron* **2012**, *31*, 607.

(30) (a) King, R. B. *Inorg. Chem.* **2006**, *45*, 8211. (b) King, R. B.; Ghosh, S. *Theor. Chem. Acc.* **2012**, *131*, 1087.

(31) Becke, A. D.; Edgecombe, K. E. *J. Chem. Phys.* **1990**, *92*, 5397.

(32) Silvi, B.; Savin, A. *Nature* **1994**, *371*, 683.

(33) Savin, A.; Nesper, R.; Wengert, S.; Fässler, T. F. *Angew. Chem., Int. Ed.* **1997**, *36*, 1808.

(34) Nalewajski, R. F.; Mrozek, J. *Int. J. Quantum Chem.* **1994**, *51*, 187.

(35) Fehlner, T. P. *Collect. Czech. Chem. Commun.* **1999**, *64*, 767.

(36) Scientific Computing and Modeling (SCM). ADF2010.02. In *Theoretical Chemistry*; Vrije Universiteit: Amsterdam, The Netherlands, http://www.scm.com.

(37) te Velde, G.; Bickelhaupt, F. M.; Baerends, E. J.; van Gisbergen, S. J. A.; Fonseca Guerra, C.; Snijders, J. G.; Ziegler, T. *J. Comput. Chem.* **2001**, *22*, 931.

(38) Vosko, S. H.; Wilk, L.; Nusair, M. *Can. J. Phys.* **1980**, *58*, 1200.
(39) Becke, A. D. *J. Chem. Phys.* **1986**, *84*, 4524.
(40) Becke, A. D. *Phys. Rev. A* **1986**, *38*, 3098.
(41) Perdew, J. P. *Phys. Rev. B* **1986**, *33*, 8822.
(42) Versluis, L.; Ziegler, T. *J. Chem. Phys.* **1988**, *88*, 322.
(43) (a) van Lenthe, E.; Baerends, E. J.; Snijders, J. G. *J. Chem. Phys.* **1993**, *99*, 4597. (b) van Lenthe, E.; Baerends, E. J.; Snijders, J. G. *J. Chem. Phys.* **1994**, *101*, 9783. (c) van Lenthe, E.; van Leeuwen, R.; Baerends, E. J.; Snijders, J. G. *Int. J. Quantum Chem.* **1996**, *57*, 281.
(44) (a) Becke, A. D. *Phys. Rev. A* **1988**, *38*, 3098. (b) Lee, C.; Yang, W.; Parr, R. G. *Phys. Rev. B* **1988**, *37*, 785. (c) Becke, A. D. *J. Chem. Phys.* **1993**, *98*, 5648.
(45) London, F. *J. Phys. Radium* **1937**, *27*, 397.
(46) Ditchfield, R. *Mol. Phys.* **1974**, *27*, 789.
(47) Wolinski, K.; Hinton, J. F.; Pulay, P. *J. Am. Chem. Soc.* **1990**, *112*, 8251.
(48) Friedrich, K.; Seifert, G.; Grossmann, G. *Z. Phys. D (Amsterdam, Neth.)* **1990**, *17*, 45.
(49) Schreckenbach, G.; Ziegler, T. *J. Phys. Chem.* **1995**, *99*, 606.
(50) Schreckenbach, G.; Ziegler, T. *Int. J. Quantum Chem.* **1997**, *61*, 899.
(51) Schreckenbach, G.; Ziegler, T. *Int. J. Quantum Chem.* **1996**, *60*, 753.
(52) Wolff, S. K.; Ziegler, T. *J. Chem. Phys.* **1998**, *109*, 895.
(53) Wolff, S. K.; Ziegler, T.; van Lenthe, E.; Baerends, E. J. *J. Chem. Phys.* **1999**, *110*, 7689.
(54) Altomare, A.; Burla, M. C.; Camalli, M.; Cascarano, G.; Giacovazzo, C.; Guagliardi, A.; Moliterni, A. G. G.; Polidori, G.; Spagna, R. *J. Appl. Crystallogr.* **1999**, *32*, 115.
(55) Sheldrick, G. M. *Acta Crystallogr., Sect. A: Found Crystallogr.* **2008**, *A64*, 112.
(56) Farrugia, L. J. *J. Appl. Crystallogr.* **1999**, *32*, 837.
(57) *SHELXS-97*; Sheldrick, G. M. University of Göttingen: Germany, 1997.
(58) *SHELXL-97*; Sheldrick, G. M. University of Göttingen: Germany, 1997.